ENVISAT ASAR POLARIZATION EXPERIMENT IN PETER THE GREAT BAY, JAPAN SEA: PRELIMINARY RESULTS

Leonid M. Mitnik, Vyacheslav A. Dubina and Oleg G. Konstantinov

Department of Satellite Oceanography, V.I. Il'ichev Pacific Oceanological Institute, FEB RAS, Vladivostok, Russia; e-mail: mitnik(at)poi.dvo.ru

ABSTRACT

A series of ASAR images with alternating polarization was acquired over Peter the Great Bay, Japan Sea in 2003-2005. A combination of horizontal-horizontal (*HH*) and vertical-vertical (*VV*) polarization was used with two different mean incidence angles θ = 18.3° and 22.5°. Additionally, the same scenes were sensed on 23 September 2004 by ERS-2 SAR with a delay of about 30 min after the ASAR acquisition. The main aim was to study the polarimetric signatures of the sea surface caused by the oceanic dynamic phenomena as well as by natural and anthropogenic slicks for later use for their detection and classification. During the ASAR and SAR data acquisitions, ground-truth measurements of the sea surface temperature, wind speed and direction as well as polarization images of the sea surface recorded by a polarization video system were arranged at POI Marine Stations and at several coastal points. Wind fields were also retrieved from the SAR images using the CMOD-4 scatterometer algorithm. As a rule, the wind speed during the satellite observations did not exceed 7 m/s so that radar signatures of slicks, eddies, currents, and internal waves were revealed on the SAR images. The *HH* and *VV* radar cross-sections σ_{oHH} and σ_{oVV} computed from ASAR data decreased with θ and the polarization ratio $P = \sigma_{oVV}/\sigma_{oHH}$ increased. Variations of *P* in the area around the slicks reached 2-4 dB which calls for further investigations.

Keywords: Envisat ASAR, ESR-2 SAR, polarimetric signatures, radar signatures of oceanic phenomena.

INTRODUCTION

Among the new specificities of the Envisat ASAR, the polarization diversity makes the instrument very promising. The Alternating Polarization (*AP*) mode provides two simultaneous images from the same area with three possible polarization combinations: *HH* and *VV*, *HH* and *HV*, *VV* and *VH* with high spatial resolution as in the single polarization mode but with degraded radiometric resolution. There is considerable interest in the *AP* mode for oceanic dynamic phenomena detection against the variable background. From current research using airborne real aperture radar or synthetic aperture radar data, it follows that a combination of *VV* and *HH* polarizations allows discrimination of surface imprints of atmospheric and oceanic phenomena. Experimental results indicate that oceanic features (internal waves, fronts, eddies, etc.) tend to appear somewhat better with *HH* than with *VV* polarization. In contrast, sea surface imprints of atmospheric features (fronts, convective cells and rolls, etc.) appear to be more visible with *VV* polarization than with *HH* polarization. Films of surfactants both natural (mainly biogenic) and man-made (mainly oil spills) have manifested themselves on satellite SAR images in a form of dark bands and patches at any polarization when wind speed W < 6-7 m/s (1,2). These films can serve as an indicator of oceanic dynamic processes like fronts, currents, eddies, upwellings, internal waves, etc. both at *VV* and *HH* polarization. In connection with this, an advantage of alternating polarization data over one polarization in phenomena/background discrimination should be studied in a wide range of sensing geometry and environmental parameters variations.

METHODS

Envisat ASAR and ERS-2 SAR sensing of Peter the Great Bay, Japan Sea was carried out in different seasons. The boundaries of SAR frames and the location of POI Marine Stations and of the Far Eastern Marine Reserve are sketched in Figure 1a. The area of the Cape Shults Marine station where measurements of the sea surface roughness with a polarization spectrophotometer were performed and artificial slicks were created from a yacht is depicted in Figure 1b.

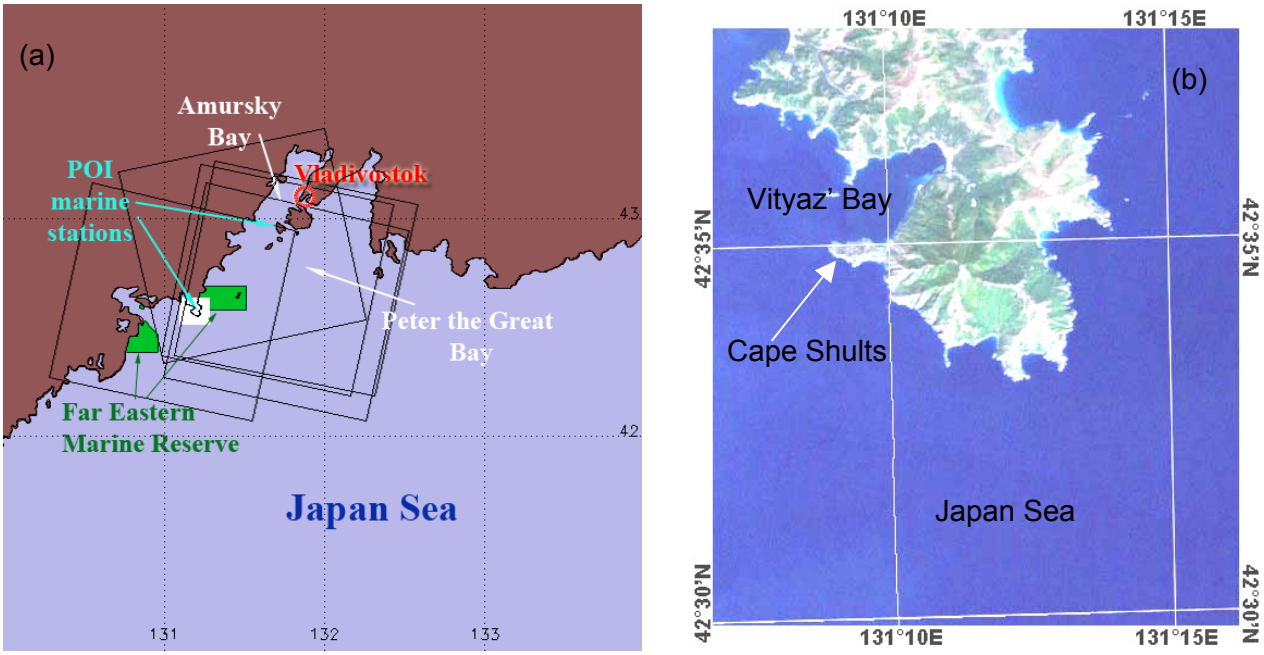

Figure 1: (a) Map of Peter the Great Bay with the boundaries of Envisat ASAR and ERS-2 SAR images used in the study. Arrows indicate the location of POI Marine stations and the Far Eastern Marine Reserve. (b) Cape Shults Marine Station, Vityaz' Bay and the open regions of the Japan Sea where in situ *data were collected and experiments with artificial slicks were conducted.*

Table 1 presents the satellite title, the date and time of acquisition, *in situ* data near Cape Shults (wind speed and direction, air-sea temperature difference $\Delta T_{as} = T_a - T_s$, where T_a is the air temperature near the sea surface and T_s is the sea surface temperature), as well as the incidence angle θ of the Cape Shults area and the values of the Normalized Radar Cross Section (*NRCS*) at *V* and *H* polarizations σ_o^{VV} and σ_o^{HH} to the south of Cape Shults. Local time is equal to Greenwich time plus 10 hours.

Table 1: Envisat ASAR VV- and HH-polarization images taken over Peter the Great Bay.

SAR product	Date	Time (UTC)	Wind speed W / m/s	Wind direction /deg	ΔT_{as} /°C	Incidence angle θ /deg	σ_{oVV} /dB	σ_{oHH} /dB
ASAR AP	2003-09-20	01:33	3.0-5.0	310	-2.8	21.7	-5.8	-6.4
ASAR AP	2004-05-06	01:36	6.0-7.0	180	5.0	17.5	-0.5	-2.0
ASAR AP	2004-07-12	01:30	3.5-4.0	135	0.3	25.8	-10.3	-13.1
ASAR AP	2004-07-15	01:36	3.0-3.5	225	0.3	17.5	-6.6	-8.8
ASAR AP	2004-09-20	01:30	3.0-4.0	320	-2.9	25.8	-12.4	-14.9
SAR PRI	2004-09-20	01:59	3.0	300	-2.1	26.0	-6.3	
ASAR AP	2004-09-23	01:36	2.0-3.0	315	-2.9	17.5	-4.0	-5.3
ASAR AP	2004-09-23	12:54	4.0	180	-2.0	15.9	-1.1	-1.9
ASAR AP	2005-02-10	12:54	9.0	315	-11.8	15.9	3.2	2.3
ASAR AP	2005-02-26	01:33	6.0	315	-14.0	21.7	-3.8	-4.9

Data processing

The *NRCS* values were computed for the square areas at the size of 100 m × 100 m for each ASAR/SAR image using the BEST tool (3). The values σ_o^{HH} and σ_o^{VV} given in Table 1 were determined in areas with a uniform brightness distribution near Cape Shults in cells of 1 km × 1 km.

CMOD4, the most commonly used scatterometer algorithm, is described by the function (4):

$$\sigma_o^{VV} = a(\theta) W^{\gamma(\theta)} \left(1 + b(\theta)\cos\varphi + c(\theta)\cos 2\varphi\right) \quad (1)$$

where θ is the local incident angle, $\gamma(\theta)$ is the power law dependence on wind speed, and φ is the angle between the radar looking direction and the wind direction. It was used for wind speed retrieval when information on wind direction was available (usually it was assumed that the wind speed *W* is measured at 10 m above the surface with neutral atmospheric stability).

Wind fields were also retrieved from the measured σ_o^{HH} values using the CMOD4 algorithm and a polarization ratio equation suggested by Thompson et al. (5) and Thompson and Beal (6):

$$\frac{\sigma_o^{HH}}{\sigma_o^{VV}} = \frac{(1 + \alpha \tan 2\theta)^2}{(1 + 2\tan 2\theta)^2} \quad (2)$$

By varying the parameter α a value, α_{opt} can be found that provides the best correspondence of wind fields retrieved from σ_o^{VV} and from σ_o^{HH}; $\alpha = 0$ corresponds to the polarization ratio predicted by Bragg scattering and $\alpha = 2$ to the CMOD4 case.

The polarization ratio $P = \sigma_o^{VV} / \sigma_o^{HH}$ was computed to reveal its changes caused by modulation of the sea surface roughness by oceanic dynamic phenomena at different incidence angles.

RESULTS

Wind fields

The Envisat ASAR image with *VV* polarization acquired from the descending orbit 12367 on 12 July 2004 is shown in Figure 2a. The image covers 100 km × 100 km centred around 42°40'N, 131°50'E. The incidence angle varied between 18.7° and 26.2° over the image. The wind field was retrieved from σ_o^{VV} values using the scatterometer algorithm (1). The *W* values vary from 2 to 7 m/s (Figure 2b). Wind speed measurements at several coastal points in the Peter the Great Bay and on a yacht in Vityaz' Bay, and south of Cape Shultz (Figure 1) confirm the satellite estimates.

Wind speed values retrieved from *HH* polarization images were generally larger than those from the *VV* polarization at all values of parameter α. The average difference reached 3.7 m/s at $\alpha = 0.6$ (determined from RADARSAT data) and decreased to 1.67 m/s at $\alpha = 2.0$.

Slicks

There are several slick bands and patches on the image which are distinguished from the surrounding waters by a dark tone. The variations of the NRCS with *VV* and *HH* polarizations along section A crossing the biogenic slicks and section B crossing an oil slick are given in Figure 3a,b. The profiles were computed by averaging 11 pixels at the size of 25 m × 25 m with a moving average of seven pixels. The damping degree (contrast) reached 10-15 dB for biogenic slicks both on *VV* and on *HH* polarizations. With the oil slick the contrast against the surrounding waters was only 3-4 dB which was very likely due to 'the age' of the slick.

Slicks were also detected on other SAR images taken when the wind speed W ≤ 5 m/s. However, at higher winds as observed on 6 May 2004, 10 and 26 February 2005 (Table 1) biogenic slicks

disappeared. During winter, not only biogenic slicks but also slick-like dark features were observed in Peter the Great Bay near the ice edge caused by grease ice.

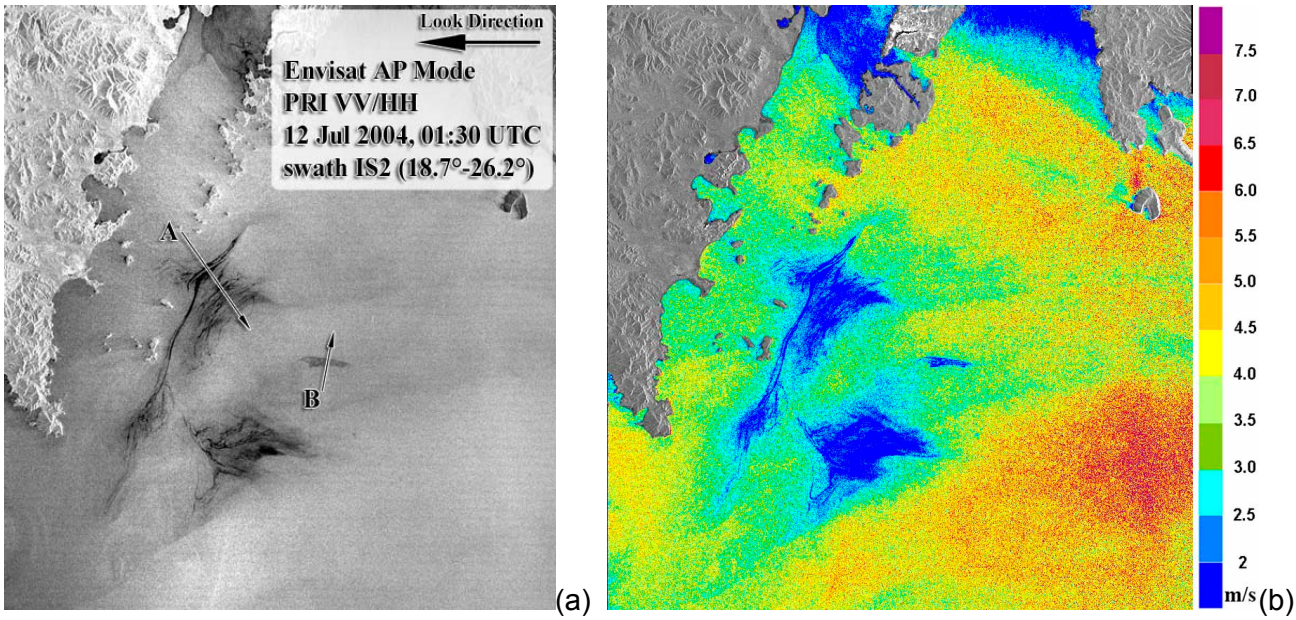

Figure 2: (a) Envisat ASAR image of Peter the Great Bay acquired on 12 July 2004 at 01:30 UTC with VV polarization (b) and surface wind field derived from the NRCS values with the scatterometer function (1). Biogenic slicks and oil spill damp the small-scale roughness and wind retrieval becomes impossible. The slick-covered areas (at the bottom left) as well as the areas with W ≤ 2 m/s have a dark tone in Figure 2a and a blue tone in Figure 2b. Arrows A and B refer to the NRCS profiles shown in Figure 3.

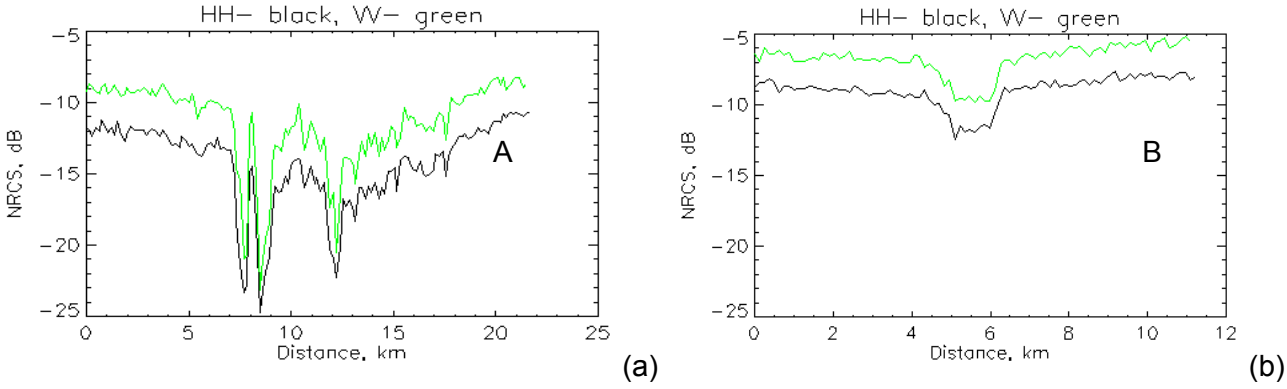

Figure 3: Profiles of NRCS across (a) biogenic slicks and (b) an oil spill at vertical (green lines) and horizontal (dark lines) polarizations along sections A and B shown in Figure 2a.

We considered the variations of the polarization ratio $P = \sigma_o^{VV} / \sigma_o^{HH}$ in the area covered by biogenic slicks depicted on a fragment of the ASAR image at a size of 20 km × 20 km (Figure 4a). The average incidence angle for the fragment is 22°. The wind speed around the slick area varied from 2.5 to 4 m/s (Figure 2b). At first, the *NRCS* values at *VV* and *HH* polarization were computed for the whole image pixel by pixel of size 25 m × 25 m. Then *NRCS* profiles were determined for three sections, A, B and C, each representing a band 21 pixels wide. The location of sections and their directions are marked by arrows in Figure 4a. The direction of the sections was mainly normal to the slick bands. At last, polarization ratio profiles were calculated for each section as the ratio of the average *NRCS* values at *VV* and *HH* polarizations subject to a moving average along the section with a window width of seven pixels. The *P* profiles are given in Figures 4b,c and d. Dark vertical lines mark the location of the individual narrow or wide slick bands.

The polarization ratio along profiles is characterised by large variations. The largest changes are typically (but not always) observed near the slick bands.

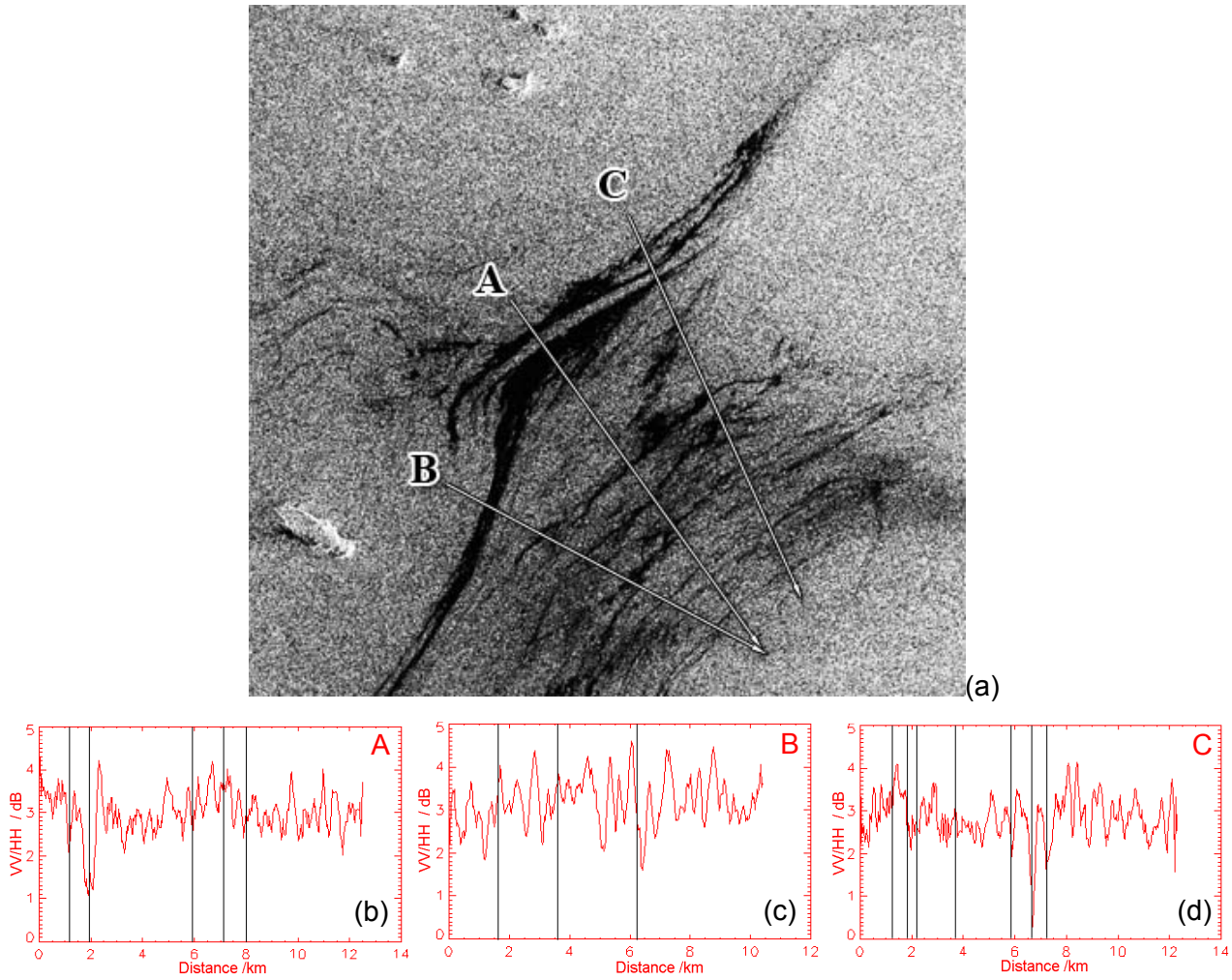

Figure 4: (a) a fragment of Envisat ASAR image for 12 July 2004 with plentiful filamentary slicks. Arrows indicate direction of sections A, B and C for which polarization ratio profiles (b), (c) and (d) were computed.

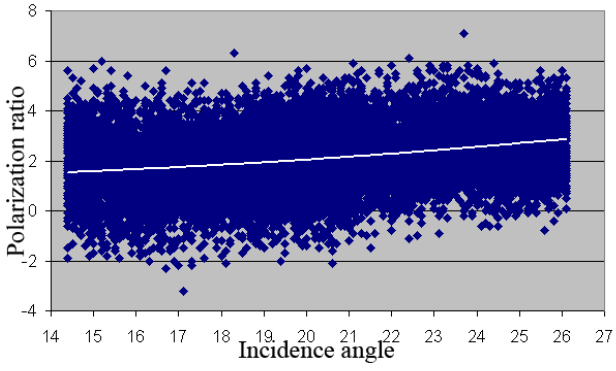

Figure 5: Dependence of polarization ratio on incidence angle.

The polarization ratio as a function of incidence angle was computed from ASAR data obtained on 12 and 15 July 2004 at a wind speed ranging between 3 and 5 m/s (about 60,000 points). The corresponding points were selected from wind fields such as shown in Figure 2b for 12 July. Each point in Figure 5 defines the *P* value for an area of the size of 100 m × 100 m. The average *P* values increase from about 1.5 dB at $\theta = 14.5° - 15°$ ° to 2.8 at $\theta = 25.5° - 26°$. The increase of *P*

with incidence angles confirms the data by Mouche et al. (7). Deviations from the average values (white line in Figure 5) are important: *rms* is 1.14 dB at $\theta = 19° - 21°$ and 1.03 dB at $\theta = 24° - 26°$.

Roughness parameters were retrieved from displacements of light floats on the sea surface. The displacements were determined by processing the series of images recorded by an optical video system during Envisat ASAR image acquisition (8).

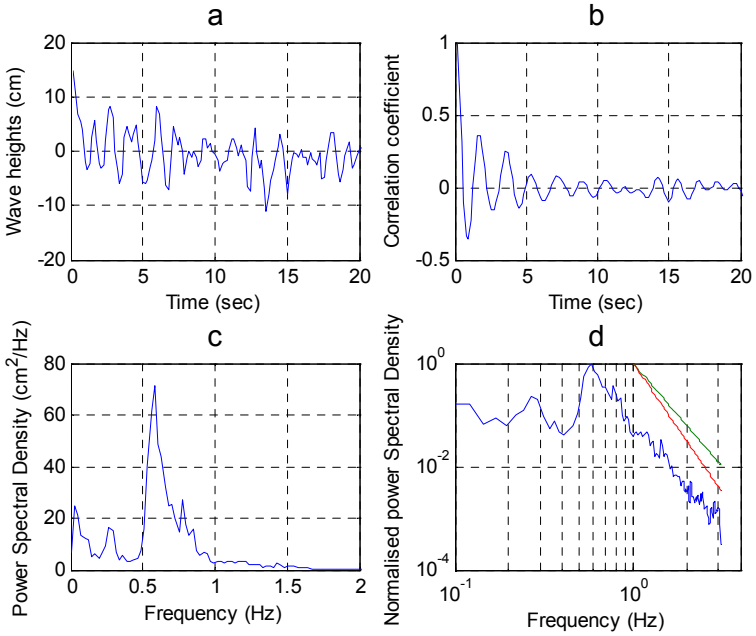

Figure 6: (a) retrieved wave height, (b) correlation function, (c) power spectral density and (d) normalised power spectral density computed for a realisation consisting of 2000 points. The slope of the green line is $\alpha = -4$ and the slope of red line is $\alpha = -5$. Measurements were conducted on 12 July 2004 at 1:30 UTC during Envisat ASAR sensing.

Indication of oceanic dynamic phenomena

Surface manifestations of internal waves were often observed on ERS-1/2 SAR and Envisat ASAR images covering both the coastal zone and the open Japan Sea (9). Their parameters estimated by processing the data obtained by coastal mooring stations as well as by satellite sensors varied in a wide range. Figure 7 shows an Envisat ASAR image acquired on 23 September 2004 at 01:36 UTC. A narrow dark band, very likely a local atmospheric front, crosses the image almost diagonally. Surface imprints of oceanic internal waves moving on shore are distinguished in the south-eastern part of the image. Front parts of the individual waves are brighter than the background in contrast to their rear parts which are darker than the background. The intensity of internal waves is high enough to produce clear imprints in the dark areas where small-scale surface waves are absent. The NRCS profiles at *VV* and *HH* polarizations as well as polarization ratio profiles were computed for sections A and B. They are presented in Figures 7b-e. Internal waves in the area under study were also detected on Terra and Aqua MODIS 250-m resolution images acquired on 22 September. Riverine waters often form fronts dividing them from marine waters and biogenic slicks on the sea surface. Elongated slick originating from a river in Vityaz' Bay was recorded by a coastal video system (8). The same slick was clearly identified on Envisat ASAR *VV*- and *HH*-polarization images (Figure 8).

Similar results were obtained for other polarization ASAR images with wind speeds not exceeding about 6-7 m/s which is favourable for the detection of surface manifestations of dynamic oceanic phenomena as well as natural slicks and oil spills (1,2). In winter, the wind speed was, as a rule, higher than in summer, thus hindering observation of oceanic dynamics and slicks. However, at wind speeds less than 6-7 m/s radar signatures of eddies of different size, frontal boundaries and slicks were observed in the subarctic frontal zone in the Japan Sea between 41 and 43°N. The features of SAR images were well correlated with SST distribution (10).

Apart from slicks, the damping of sea surface roughness in winter was caused by the grease ice in Peter the Great Bay. It is suggested that polarization differences will be higher at larger incidence angles, The corresponding experiments shall be conducted in July-October using bands 4-7 within the ASAR wide swath for which $\theta = 31° - 45.2°$.

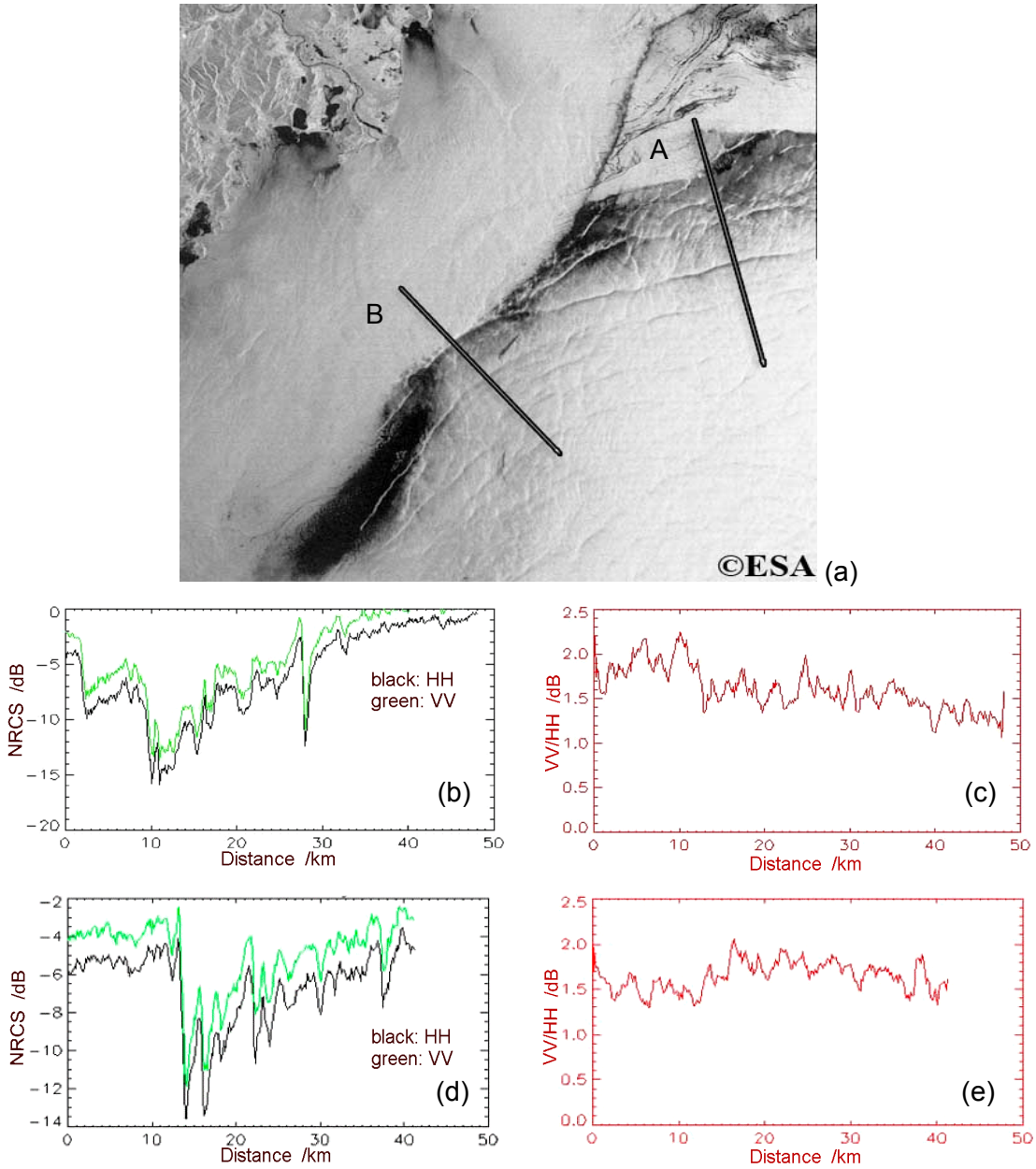

Figure 7: (a) Envisat ASAR image at VV-polarization of the south-western part of Peter the Great Bay for 23 September 2004 at 01:36 UTC showing atmospheric front and a packet of oceanic internal waves propagating onshore. Dark lines mark the location of sections A and B. NRCS profiles at VV *(green lines) and* HH *(dark lines) polarizations (b) and (d), and polarization ratio profiles (c) and (e) along sections A (b and c) and B (d and e).*

CONCLUSIONS

A series of the ASAR images with *VV*- and *HH*-polarization was acquired over Peter the Great Bay, Japan Sea both in warm and cold seasons in 2003-2005. Ground truth data including the measurements of the sea surface roughness were collected during satellite sensing and used to interpret ASAR signatures. The oceanic dynamic phenomena were revealed both on *VV*- and *HH*-polarization images in particular when there were slicks on the sea surface. Sea surface wind

fields were retrieved with a C-band scatterometer function and the variations of a polarization ratio were determined in the areas covered by surface films as well as in the areas where surface imprints of oceanic internal waves were detected. The available data do not allow to conclude whether *VV*- or *HH*-polarization or their combination is generally better for studying oceanic phenomena. Likely it is due to the small incidence angles with average values of 18.3° or 22.5°. However, one cannot rule out the influence of calibration errors, pointing accuracy and polarization isolation on the *VV*- and *HH*-polarization data. In connection with this, attention should be paid to the analysis of ASAR Alternating Polarization Mode Complex images (product ID ASA_APS_1P) and to the development of software for processing this product.

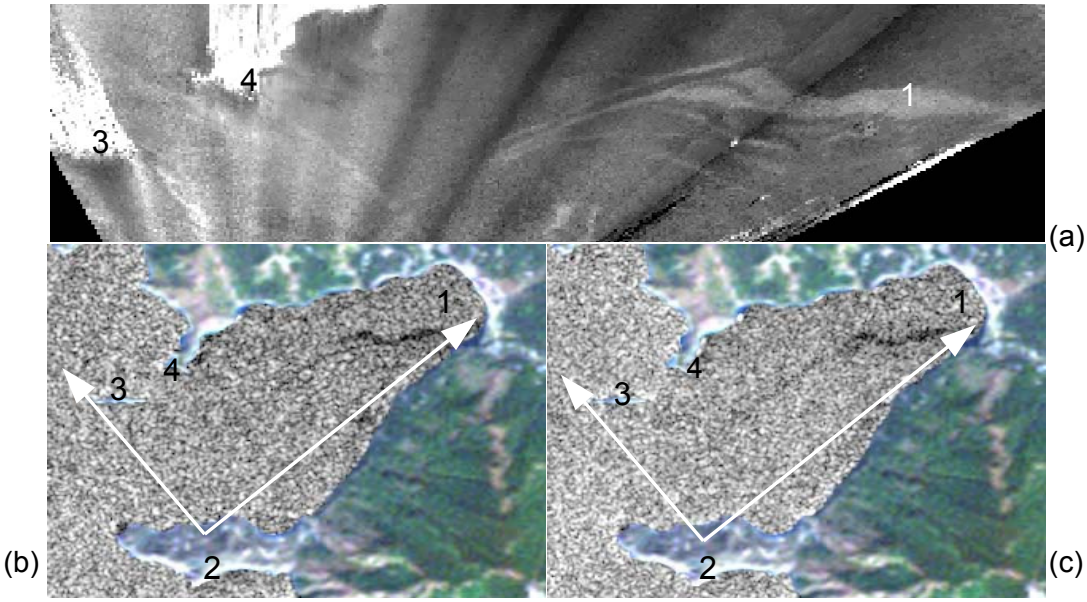

Figure 8: (a) Panoramic image of Vityaz' Bay taken by a coastal video system from Cape Shults (2) and transformed on a plane. The light elongated band of variable width is a biogenic slick (1). Envisat ASAR images of Vityaz' Bay for 20 September 2003 at (b) VV *and (c)* HH *polarization. The biogenic slick has a dark tone on both images, however there are differences in its appearance. (3) two small islands, (4) cape on the northern coast of Vityaz' Bay. White arrows show the boundaries of field of view of coastal video camera.*

ACKNOWLEDGEMENTS

This study has been carried out within ESA projects AO3-401 and AO-ID-391 and an international project BE.2775 *Detection and parameter estimation of organic pollution in the coastal zone* (DeCOP). This work is partly supported by INTAS Project 03-51-4987 *Slicks as Indicators of Marine Processes* (SIMP) and by the Russian Fund of Basic Research through Project 06-05-96076_p_vostok_a. We also thank two anonymous referees whose comments led to a substantial improvement of the paper.

REFERENCES

1 Ermakov S A, S G Salashin & A R Panchenko, 1992. Film slicks on the sea surface and some mechanisms of their formation. Dynamics of Atmospheres and Oceans, 16: 279-304

2 DiGiacomo P M & H Benjamin, 2001. Satellite observations of small coastal ocean eddies in the Southern California Bight. Journal of Geophysical Research, 106: 22521-22544

3 http://envisat.esa.int/services/best/

4 Stoffelen A C M & D L T Anderson, 1997. Scatterometer data interpretation: Estimation and validation of the transfer function: CMOD4. Journal of Geophysical Research, 102: 5767-5780

5 Thompson D R, T M Elfouhaily & B Chapron, 1998. Polarization ratio for microwave backscattering from the ocean surface at low to moderate incidence angles. In: Proc. International Geoscience and Remote Sensing Symposium (Seattle, WA), 1671-1676

6 Thompson D R & R C Beal, 2000. Mapping high-resolution wind fields using synthetic aperture radar. The Johns Hopkins Univ. Tech. Dig., 21: 58-67

7 Mouche A, D Hauser, V Kudryavtsev & J-F Daloze, 2005. Multi-polarization ocean radar cross-section from ENVISAT, and airborne polarimetric radar measurements. In: 2004 Envisat & ERS Symposium (Salzburg, Austria) ESA SP-572

8 Konstantinov O G, 2005. Analysis of polarizing video images of the sea surface. In: 2nd EARSeL Workshop on Remote Sensing of the Coastal Zone (Porto, Portugal), Abstract Book

9 Mitnik L M, H-J Yoon, V A Dubina, Y-S Kim & S-W Kim, 2003. ERS SAR observations of the Korean coastal waters. In: The 24th Asian Conference on Remote Sensing & 2003 International Symposium on Remote Sensing (Busan, Korea), 1: 228-230

10 Mitnik L M & V A Dubina, 2005. Synoptic-scale, mesoscale and fine-scale oceanic features in the Japan/East Sea: Study with ERS-1/2 SAR and Envisat ASAR. In: Proc. International Geoscience and Remote Sensing Symposium (Seoul, Korea), Vol. VII: 4788-4791